doi:10.1111/evo.13898

Macroevolution of desiccation-related morphology in plethodontid salamanders as inferred from a novel surface area to volume ratio estimation approach

Erica K. Baken,[1,2] Lauren E. Mellenthin,[3] and Dean C. Adams[1]

[1] *Department of Ecology, Evolution, and Organismal Biology, Iowa State University, Ames, Iowa 50011*

[2] *E-mail: erica.baken@gmail.com*

[3] *Department of Ecology and Evolutionary Biology, Yale University, New Haven, Connecticut 06520*

Received September 9, 2019

Accepted November 18, 2019

Evolutionary biologists have long been interested in the macroevolutionary consequences of various selection pressures, yet physiological responses to selection across deep time are not well understood. In this paper, we investigate how a physiologically relevant morphological trait, surface area to volume ratio (SA:V) of lungless salamanders, has evolved across broad regional and climatic variation. SA:V directly impacts an organisms' ability to retain water, leading to the expectation that smaller SA:Vs would be advantageous in arid, water-limited environments. To explore the macroevolutionary patterns of SA:V, we first develop an accurate method for estimating SA:V from linear measurements. Next, we investigate the macroevolutionary patterns of SA:V across 257 salamander species, revealing that higher SA:Vs phylogenetically correlate with warmer, wetter climates. We also observe higher SA:V disparity and rate of evolution in tropical species, mirrored by higher climatic disparity in available and occupied tropical habitats. Taken together, these results suggest that the tropics have provided a wider range of warmer, wetter climates for salamanders to exploit, thereby relaxing desiccation pressures on SA:V. Overall, this paper provides an accurate, efficient method for quantifying salamander SA:V, allowing us to demonstrate the power of physiological selection pressures in influencing the macroevolution of morphology.

KEY WORDS: **Macroevolution, salamander, surface area to volume ratio.**

Evolutionary biologists have long sought to identify the relationship between ecological selective pressures and phenotypic variation. Comparative analyses have been particularly fruitful to this end, having demonstrated a clear association between phenotypic variation and ecological selection gradients in various taxa. This includes such classic examples as limb length variation across locomotive constraints in *Anolis* lizards (Losos 1992), cryptic coloration matching environmental backgrounds in pocket mice (Hoekstra et al. 2004), and body shape differences associated with benthic and limnetic habitats in stickleback fishes (Schluter and McPhail 1992). These and other studies offer strong evidence for the power of natural selection in promoting phenotypic diversity, and provide the basis of our understanding of phenotypic macroevolution.

It is important to note, however, that these comparative studies have historically concentrated on specific components of the phenotype, while other vital traits have been relatively neglected. Specifically, much is known about how ecological selection pressures influence traits related to biomechanics (e.g., jaw strength in labrid fishes, Wainwright 1988), species interactions (e.g., armoring in sticklebacks, Moodie 1972), and reproductive success (e.g., horn complexity in scarab beetles, Emlen et al. 2007), whereas physiological traits are rarely studied on a macroevolutionary scale (Gifford 2016, but see Blomberg et al. 2003; Lane et al.

© 2019 The Authors. *Evolution* © 2019 The Society for the Study of Evolution.

2004; Grigg and Buckley 2013). Consequently, how physiological traits respond to ecological selective pressures across deep time remains obscure.

In an effort to expand our knowledge of these recondite evolutionary processes, we herein examined how a physiologically relevant trait in salamanders (surface area to volume ratio [SA:V]) has evolved across multiple axes of ecological variation on a macroevolutionary scale. Across organisms, a high SA:V confers several physiological consequences, including increased risk of desiccation. Salamanders are well known for their vulnerability to desiccation, as their permeable skin provides little resistance to water loss (MacMahon 1964; Spight 1968; Spotila and Berman 1976). When exposed to arid environments, fatal desiccation can occur in some lungless salamanders (family: Plethodontidae) in less than 1 hour (Ray 1958), suggesting that desiccation acts as a strong selective pressure in this family. Previous research has shown species diversification rates and species richness are correlated with patterns of climatic niche evolution (Kozak and Wiens 2010, 2016), potentially implicating the threat of environmentally induced desiccation as a macroevolutionary force in Plethodontidae. Additionally, several ecological studies have demonstrated that plethodontids mitigate desiccation risk through a suite of physiological, behavioral, and microhabitat selection responses (Spotila 1972; Fraser 1976; Feder and Londos 1984; Riddell and Sears 2015; Farallo et al. 2018). Although salamanders can employ these strategies to temporarily lower desiccation rates, the ultimate arbiter of baseline desiccation rate is SA:V (MacMahon 1964). As lungless salamanders depend solely on cutaneous respiration, SA:V also constrains rates of oxygen consumption, metabolism, and, therefore, activity patterns (Ultsch 1976). When viewed from this perspective, we considered SA:V to be one of the most ecologically and physiologically relevant traits for this family.

Because of its role in desiccation and respiration, SA:V has been implicated as the basis of numerous ecological patterns observed in the family Plethodontidae. For instance, McEntire (2016) and McEntire and Maerz (2019) suggested that SA:V correlates negatively with the frequency and duration of climbing behavior. Differences across juvenile and adult dispersal, microhabitat use, surface activity, and physiology are also thought to be driven by the ontogeny of decreasing SA:V across life stages (Sattler and Reichenbach 1998; Rittenhouse et al. 2004; Riedel et al. 2012; Peterman and Semlitch 2014). Importantly, however, none of these studies measured SA:V directly. Rather, they utilized surrogates of SA:V, such as body size (snout-vent length [SVL]) or surface area (SA) proxies derived from body mass alone, both of which assume a uniform body shape for every individual. Unfortunately, such an assumption directly contradicts empirical patterns of body shape variation in salamanders that has been observed across sizes (Hanken 1982; Wake 1989), within species (Adams 2011), and among species (Adams et al. 2009; Blankers et al. 2012; Baken and Adams 2019), as demonstrated through quantitative morphometric analyses. However, at present, we lack a direct method for efficiently quantifying SA:V variation. Consequently, the evolutionary history of this physiologically relevant trait remains obscure.

This study has two aims. First, we developed a noninvasive and accurate method of estimating SA:V for plethodontid salamanders, using 11 linear body measurements to encompass the full body shape along with geometric, volumetric, and trigonometric equations. We assessed the accuracy of our SA:V estimation method by empirically measuring SA:Vs for a subset of specimens using 3D scanning technology and volumetric displacement. We then regressed our estimates on the empirically measured SA:Vs and compared the fit of our estimates to the commonly used mass-based Whitford Hutchinson (WH) proxy.

Second, we explored macroevolutionary patterns of SA:V in a phylogenetic context via its association with various abiotic conditions in plethodontid salamanders. Following the above assertion that SA:V influences osmoregulation and respiration, we hypothesized that SA:V varies across taxa based upon variation in physiologically relevant climatic factors: precipitation, temperature, and elevation. Further, as tropical and temperate plethodontids differ substantially across several biological axes (e.g., higher diversification rate in the tropical clade, Wiens 2007; higher incidence of arboreality in the tropics, Baken and Adams 2019), we predicted that SA:V varies across geographic region as well. Thus, we hypothesized that climate and region have influenced the macroevolution of SA:V across the history of Plethodontidae. We tested this hypothesis by applying our SA:V estimation approach to 2364 specimens across 257 plethodontid species in a phylogenetic analysis of covariance (ANCOVA) framework.

Materials and Methods

DERIVING SURFACE AREA TO VOLUME RATIO (SA:V) ESTIMATES

Here, we developed an estimate of SA:V by considering the full salamander body form to be composed of three geometric shapes: an elliptical cylinder (the body), an elliptical cone (the tail), and an elliptical frustum (the head; Fig. 1B). We excluded limbs from our estimates because overall SA:V was minimally affected by their inclusion (results not shown). Calculating the SAs and volumes (Vs) for these shapes requires obtaining a set of 11 linear measurements from each specimen (Fig 1A), which were subsequently used in the equations derived below.

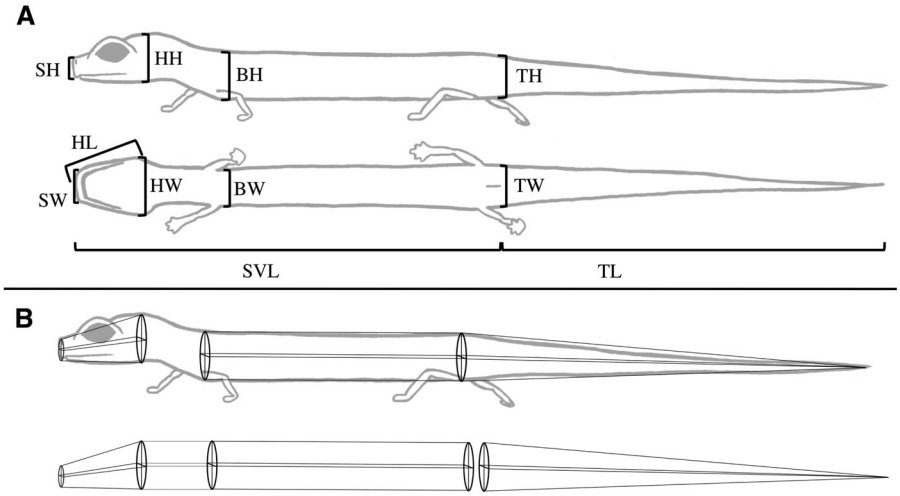


Figure 1. Specimen diagram of the morphological components quantified in this study. (A) The 11 linear measurements used to quantify surface area to volume ratio (SA:V) included snout height (SH), head height (HH), body height (BH), tail height (TH), snout width (SW), head length (HL), head width (HW), body width (BW), tail width (TW), snout-vent length (SVL), and tail length (TL). These measures are defined in Table S1. (B) SA:V was calculated by treating different body parts as different geometric shapes: an elliptical frustum (head), an elliptical cylinder (body), and an elliptical cone (tail).

First, for the body, we calculated V (eq. 1) and lateral SA (eq. 2) of an elliptical cylinder using the following equations:

$$V_{\text{Body}} = \pi \frac{\text{BW}}{2} \frac{\text{BH}}{2} (\text{SVL} - \text{HML}), \tag{1}$$

$$\text{SA}_{\text{Body}} = 2\pi (\text{SVL} - \text{HML}) \sqrt{\frac{\left(\frac{\text{BW}}{2}\right)^2 + \left(\frac{\text{BH}}{2}\right)^2}{2}} \tag{2}$$

where midline length of the head (HML) $= \sqrt{\text{HL}^2 - \left(\frac{\text{HW}}{2}\right)^2}$, and head length (HL), head width (HW), body height (BH), body width (BW), and SVL are shown in Figure 1A and defined in Table S1.

Next, for the tail, we used a modified version of the standard equations for estimating the V (eq. 3) and lateral SA (eq. 4–7) of an elliptical cone (Beyer 1981).

$$V_{\text{Tail}} = \frac{\pi \left(\frac{\text{TW}}{2}\right) \left(\frac{\text{TH}}{2}\right) \text{TML}}{3} \tag{3}$$

$$\text{SA}_{\text{Tail}} = \int_0^{2\pi} \int_0^{\text{TML}} \sqrt{\text{EG} - F^2} dx dy \tag{4}$$

$$E = \frac{\text{TLM}^2 + \left(\frac{\text{TW}}{2}\right)^2 \cos(y)^2 + \left(\frac{\text{TH}}{2}\right)^2 \sin(y)^2}{\text{TML}^2} \tag{5}$$

$$F = \frac{\left(\left(\frac{\text{TW}}{2}\right)^2 - \left(\frac{\text{TH}}{2}\right)^2\right) (\text{TML} - x) \cos(y) \sin(y)}{\text{TML}^2} \tag{6}$$

$$G = \frac{(\text{TML} - x)^2 \left(\left(\frac{\text{TW}}{2}\right)^2 \sin(y)^2 + \left(\frac{\text{TH}}{2}\right)^2 \cos(y)^2\right)}{\text{TML}^2} \tag{7}$$

where tail midline length (TML) $= \sqrt{\text{TL}^2 - \left(\frac{\text{TH}}{2}\right)^2}$, and tail width (TW), tail height (TH), and tail length (TL) are shown in Figure 1A and defined in Table S1.

Third, obtaining the SA and V for the head required treating it as an elliptical frustum (Fig. 1B). Here, we found the difference between two elliptical cones: one starting at the base of the head, extending past the snout (Full Cone) and another starting at the snout, extending to the tip of the Full Cone (Extra Cone). Subtracting the Extra Cone from the Full Cone gives the V and lateral SA of an elliptical frustum. Thus, we applied the elliptical cone equations (3–7) to both the Full and Extra Cone calculations with the following substitutions: HW and snout width (SW) replaced TW, head height (HH) and snout height (SH) replaced TH, and Full Cone midline length (FCML) and Extra Cone midline length (ECML) replaced TML. HW, SW, HH, and SH are shown in Figure 1A and defined in Table S1, and calculations for FCML and ECML can be found in the Supporting Information Materials (equations S1–S3). We calculated the SA of the top of the frustum (corresponding to the tip of the snout) with the equation for the area of an ellipse:

$$\text{SA}_{\text{SnoutTip}} = \pi \frac{\text{SW}}{2} \frac{\text{SH}}{2} \tag{8}$$

Finally, specimen-wide SA:V was calculated by combining the SA and V measures from each body part (eq. 9). R

code and data for SA:V calculations are available on Dryad (https://doi.org/10.5061/dryad.59zw3r23m).

$$\text{SA:V} = \frac{\text{SA}_{\text{Body}} + \text{SA}_{\text{Tail}} + \text{SA}_{\text{Head}}}{\text{V}_{\text{Body}} + \text{V}_{\text{Tail}} + \text{V}_{\text{Head}}} \quad (9)$$

SA:V PERFORMANCE EVALUATION

We assessed the utility of our approach using 21 specimens across a range of species and sizes. This included *Aneides ferreus* (1), *Desmognathus fuscus* (3), *Desmognathus ochrophaeus* (3), *Eurycea lucifuga* (2), *Plethodon glutinosus* (2), *Plethodon shermani-teyahalee* hybrids (9), and *Pseudotriton ruber* (1), ranging in size (SVL) from 22.46 to 76.40 mm. We recognize that the samples evaluated here do not represent the full breadth of shape diversity for the family (e.g., elongate *Batrachoseps* species). However, given that the measurements used in our proxy encompass linear dimensions that describe these shape differences (e.g., trunk and tail length relative to thickness), our proxy should provide reasonable estimates of SA:V across the family. For each specimen, we empirically measured SA:Vs using 3D scans and volumetric displacement. Next, we estimated SA:V using our linear measurement method as described above, and we estimated SA with the frequently used Whitford and Hutchinson (1967) proxy (WH) for plethodontids: $\text{SA} = 9.62(W^{0.614})$. The parameters of this proxy (9.62 and 0.614) were derived empirically (Whitford and Hutchinson 1967), and W was the preserved specimen body mass in grams. We then used linear regression and model comparison to assess the relative utility of our SA:V estimates to the log-transformed SA proxy.

MACROEVOLUTION OF SA:V

In the latter part of this study, we used our SA:V estimation approach to explore how this physiologically relevant trait has evolved across two axes of ecological diversity: climate and geographic region. Several lines of evidence inform our expectations regarding the relationship between SA:V, climate, and region. First, the rate of water loss in plethodontids is strongly influenced by SA:V, temperature, and aridity (MacMahon 1964; Spotila 1972). This would suggest that cooler, wetter climates may facilitate the survival of plethodontids with higher SA:Vs. Second, as SA:V also limits plethodontid respiratory rates (Whitford and Hutchinson 1967), the elevational gradient of available atmospheric oxygen may in turn limit SA:V evolution. Synthesizing these climatic and biological considerations, we hypothesized that SA:V responds to relaxed physiological stress in areas of low elevation, low temperatures, and high precipitation, and thus species in these climates display higher SA:Vs.

We also examined SA:V variation across regions for two reasons: the tropics are generally characterized by abiotic conditions concordant with low desiccation rates (high precipitation and humidity, Feder 1983), and the tropical clade of plethodontids is well known for its impressive ecological and evolutionary diversity (Wake 1987). Further, Kozak and Wiens (2010, 2016) suggest that climatic niche evolution may be responsible for elevated species diversification rates and species richness observed in tropical plethodontid clades. Consequently, we hypothesized that plethodontids experienced a physiological release following the invasion of the Neotropics such that tropical species display higher SA:V disparity and rate of evolution.

To address our hypotheses, we quantified SA:V for 2364 adult specimens across 257 plethodontid species (1–33 adult specimens per species, mean = 9.2). This represents a subset of specimens from Baken and Adams (2019), excluding species without publicly available geographic occurrence data and damaged specimens. Fully aquatic species were also excluded from the current study, as they only occur in temperate regions and display strong macroevolutionary patterns in body shape seemingly unrelated to climate (Bonett and Blair 2017).

To quantify the mean of climatic variables for each species, we obtained species distributional polygons from the International Union for Conservation of Nature's (IUCN) Red List of Threatened Species database (2010; 239 species polygons). We constructed 18 additional polygons following IUCN protocol from occurrence data provided by VertNet (Constable et al. 2010). We then extracted elevation (Title and Bemmels 2018) and six BioClim variables from the WorldClim database (Fick and Hijmans 2017) from each pixel within the species distribution polygons (occupied climatic landscape) and across the entire terrestrial landscape (7°S:56°N, 129°W:20°W; available climatic landscape) at a resolution of 2.5 arc-minute. BioClim variable selection was informed by previous studies of plethodontid niche variation (Currie 1991; Fisher-Reid et al. 2012; Gomez-Rodriguez et al. 2015), physiology (Spotila 1972; Gade and Peterman 2019), climatic niche evolution (Kozak and Wiens 2010), and activity patterns (Farallo et al. 2018; McEntire and Maerz 2019) to capture yearly variation in abiotic factors related to survival and behavior. These variables included Annual Mean Temperature (BIO1), Max Temperature of the Warmest Month (BIO4), Minimum Temperature of the Coldest Month (BIO5), Annual Precipitation (BIO12), Precipitation of the Wettest Quarter (BIO16), and Precipitation of the Driest Quarter (BIO17). After obtaining species means for each climatic variable, we transformed the climate data to standardized units using standard normal deviates and performed a principal components analysis (PCA). We then extracted the first three PC axes representing >90% of total climate variation (see Results section) for use in subsequent analyses. We assigned species' regional classifications based on the position of the species distributions relative to the Tropic of Cancer. Only two species ranges crossed this boundary: *Chiropterotriton multidentatus* and *Isthmura bellii*. As these species are deeply nested

within the tropical clade (Bonett and Blair 2017) and the majority of their distribution is south of the Tropic of Cancer, we treated these lineages as having undergone recent but incomplete migrations out of the tropics and were thus classified as tropical species. A list of each species' measured specimens, regional classification, and mean climatic variables can be found in Tables S2 and S3.

To test our above hypotheses, we evaluated SA:V across climate and region with a phylogenetic ANCOVA (SA:V ~ (PC1+PC2+PC3)*Region) using phylogenetic generalized least squares (PGLS). We also compared SA:V morphological disparity, rate of SA:V morphological evolution, and climatic disparity (both summarized by species ranges and across the entire available landscape) between regions to fully elucidate the interplay of climate, region, and SA:V evolution. Rate was quantified as a phylogenetically standardized variance under Brownian motion (*sensu* Adams 2014; see also O'Meara et al. 2006). To account for the nonindependence among species, we used a multigene time-calibrated phylogeny of Caudata published by Bonett and Blair (2017; ~70% species sampling, including all target species for this study) for all PGLS analyses. Details about the phylogenetic reconstruction can be found in Bonett and Blair (2017). To ensure our results were robust to the uncertainty in phylogenetic reconstruction, we repeated all comparative analyses using the set of chronograms from the posterior distribution of Bonett and Blair (2017). We calculated *P*-values using residual randomization permutation procedures in R 3.5.1 (R Core Team 2018) with the packages `geomorph` (Adams et al. 2019) and `RRPP` (Collyer and Adams 2018, 2019).

Results

SA:V PERFORMANCE EVALUATION

Our SA:V estimates displayed a strong, positive correlation with the empirically calculated values and greatly outperformed the log-transformed WH proxy in predicting SA:V (our estimate: $R^2 = 0.954$, AIC = –40.880, Fig. 2; log of WH proxy: $R^2 = 0.860$, AIC = –5.248; ΔAIC = 35.632; Fig. S1). Furthermore, as the WH proxy estimates SA and not SA:V, the correlation between these values was negative. On the other hand, the slope and intercept of our estimates regressed against actual SA:V did not differ from 1 and 0, respectively (95% $CI_{Slope} = 0.827{:}1.023$, 95% $CI_{Int} = –0.029{:}0.253$; Fig. 2), implying that our measure exhibits a 1:1 relationship with actual SA:V. Thus, our SA:V estimation method is accurate and outperforms the method most commonly used in herpetology (WH proxy).

MACROEVOLUTION OF SA:V

The first three axes of the climate PCA encompassed approximately 94% of the total climate variability (Table 1). PC1 was positively associated with mean annual temperature, minimum temperature of the coldest month, annual precipitation, and precipitation of the wettest quarter (Table 1). The phylogenetic ANCOVA revealed a positive correlation between SA:V and climate PC1 ($F = 8.8620$, $P = 0.009$; Table 2) such that SA:V increased with warmer, wetter climates (Fig. 3B). No other terms of the model significantly explained SA:V variation ($P > 0.220$; Table 2), and this climatic relationship did not differ when repeated across the 1000 posterior chronograms (Fig. S3).

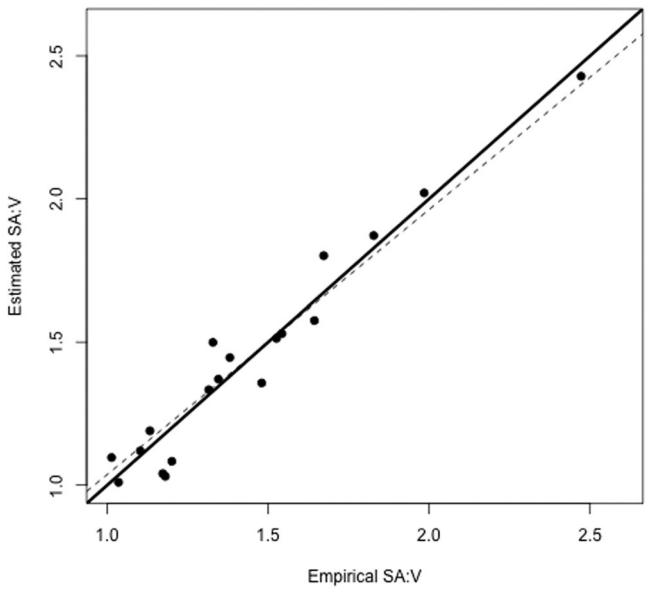


Figure 2. Linear regression of empirically measured SA:Vs and estimated SA:Vs using our novel method. Empirical SA:Vs of 21 specimens were calculated using 3D scans and volumetric displacement. The dotted line shows the correlation between the empirical and estimated SA:Vs ($R^2 = 0.954$, intercept = 0.112, slope = 0.925), which does not differ statistically from a 1:1 relationship (solid line, intercept = 0, slope = 1). This regression demonstrates the accuracy of our SA:V estimation method.

The analyses comparing SA:V disparity and rate of evolution across regions provided evidence consistent with an evolutionary release experienced by the tropical species. Specifically, tropical species displayed more than twice as much morphological disparity ($Disp_{Trop} = 0.279$, $Disp_{Temp} = 0.137$, $P = 0.001$; Fig. 3B), and exhibited substantially faster rates of morphological evolution than temperate species (rate ratio = 1.526, $P = 0.016$) when taking phylogeny into consideration. In performing a similar test of disparity on the species' mean climates across regions, we observed a much broader range of climatic variation occupied by tropical species ($Disp_{Trop} = 7.118$, $Disp_{Temp} = 3.327$, $P = 0.001$), mirroring the patterns in SA:V evolution. We subsequently constructed a "phyloclimatespace" using phylomorphospace plotting methods and the pruned Bonett and Blair consensus tree (2017), illustrating that the greater climatic disparity exhibited by

Table 1. Loadings of the climatic principal components analysis.

	PC1	PC2	PC3	PC4	PC5	PC6	PC7
BIO1 (annual temperature)	**0.4668**	−0.0950	**−0.4697**	−0.2126	0.0586	0.0716	**0.7062**
BIO4 (maximum temperature)	0.1256	**−0.6043**	−0.3058	−0.0898	**−0.6308**	−0.0938	−0.3329
BIO5 (minimum temperature)	**0.4649**	0.2201	−0.3717	−0.1991	**0.4195**	−0.0224	**−0.6174**
BIO12 (annual precipitation)	**0.4945**	0.0897	0.3912	0.1312	−0.1220	**−0.7466**	0.0707
BIO16 (precipitation wet Q)	**0.4758**	0.2699	0.1592	**0.4693**	−0.3612	**0.5669**	−0.0586
BIO17 (precipitation dry Q)	0.2593	−0.3343	**0.6066**	**−0.5749**	0.1269	0.3249	−0.0294
Elevation	−0.1098	**0.6202**	−0.0368	**−0.5824**	**−0.5113**	−0.0361	0.0023
Proportion of variance	0.4592	0.3064	0.1718	0.0426	0.0183	0.0014	0.0003
Cumulative variance	0.4592	0.7656	0.9375	0.9800	0.9983	0.9997	1.0000

Proportional and cumulative variance for each PC axis is shown in the bottom rows. Loadings values are in bold if over |0.4| to emphasize heavily loading variables for each PC axis.

tropical species distributions as well as a clear delineation between the temperate and tropical species climates (Fig. 3A) such that there is no overlap of temperate and tropical species' climatic summaries. Finally, the comparison of climate variability across the entire available landscape similarly revealed greater climatic disparity in the tropical region ($Disp_{Trop} = 4.974$, $Disp_{Temp} = 3.720$, $P = 0.001$; Fig. S2). Thus, the increased climatic disparity exhibited by the tropical species' distributional means matches the broader availability of disparate climates inherently present across the tropical landscape. The results above did not differ substantially from the robustness analyses repeated across the 1000 posterior chronograms, which are summarized in the Supporting Information Materials (Fig. S4).

Discussion

Although the macroevolutionary patterns of biomechanical traits responding to ecological selective pressures have been studied extensively, comparable patterns of physiological trait evolution are less well understood. In this study, we explored the macroevolutionary relationship of physiology, morphology, and climate by quantifying SA:Vs across the family of lungless salamanders, Plethodontidae. To do so, we first established a reliable method for estimating salamander SA:V from linear measures. We demonstrated the accuracy of this novel method by contrasting the performance of our method against the frequently used WH SA proxy in predicting actual SA:Vs across various species and sizes (Fig. 2). Using our superior method, we then examined the patterns of SA:V evolution across climatic and regional variation. We found a significant positive correlation of SA:V with warmer, wetter climates (Fig. 3B). Additionally, we found that tropical species displayed greater SA:V disparity and faster rates of SA:V evolution than temperate species (Fig. 3B). Interestingly, this regional pattern in morphological disparity was mirrored by greater climatic disparity among tropical species' distributions (Fig. 3A) and greater climatic disparity across the entire available tropical landscape (Fig. S2). Together, these patterns suggest that the tropical region inherently contains a broader array of climatic niches to exploit, providing plethodontids with a potential evolutionary release from physiological constraints following their invasion of the Neotropics. This study is the first to quantify the macroevolutionary patterns of SA:V across Plethodontidae, demonstrating the importance of accurate SA:V estimation and the impact of physiology on the evolution of plethodontid phenotypic variation.

An important note from our macroevolutionary study is that we examined broad-scale climatic factors across species ranges rather than fine-scale occurrence-based environmental measurements. We acknowledge that broad-scale climatic patterns may not directly represent what an individual salamander experiences (Ficetola et al. 2018), as plethodontids are known for small-scale movements to achieve specific microenvironmental conditions (Farallo et al. 2018). Consequently, our approach was not an attempt to quantify these selected microenvironments, but rather to characterize the broader climatic envelope that determines the frequency and variety of microenvironments available for selection. The clear correlation between SA:V and the climatic data used here only serves to emphasize the substantial influence climate has on the macroevolution of plethodontid salamanders. One limitation to this interpretation is that our findings were based on contemporary rather than historical climate data. Thus, the climate experienced by current tropical species may not represent what species experienced during the invasion of the Neotropics 45 MYA (Shen et al. 2016). Due to the limitations of the data, we did not attempt to define the environmental conditions at any particular point in history.

Somewhat surprisingly, this study revealed a positive correlation between SA:V, precipitation, and temperature (Table 2, Fig. 3B). While SA:V's positive relationship with precipitation follows logically (high SA:V corresponds with high

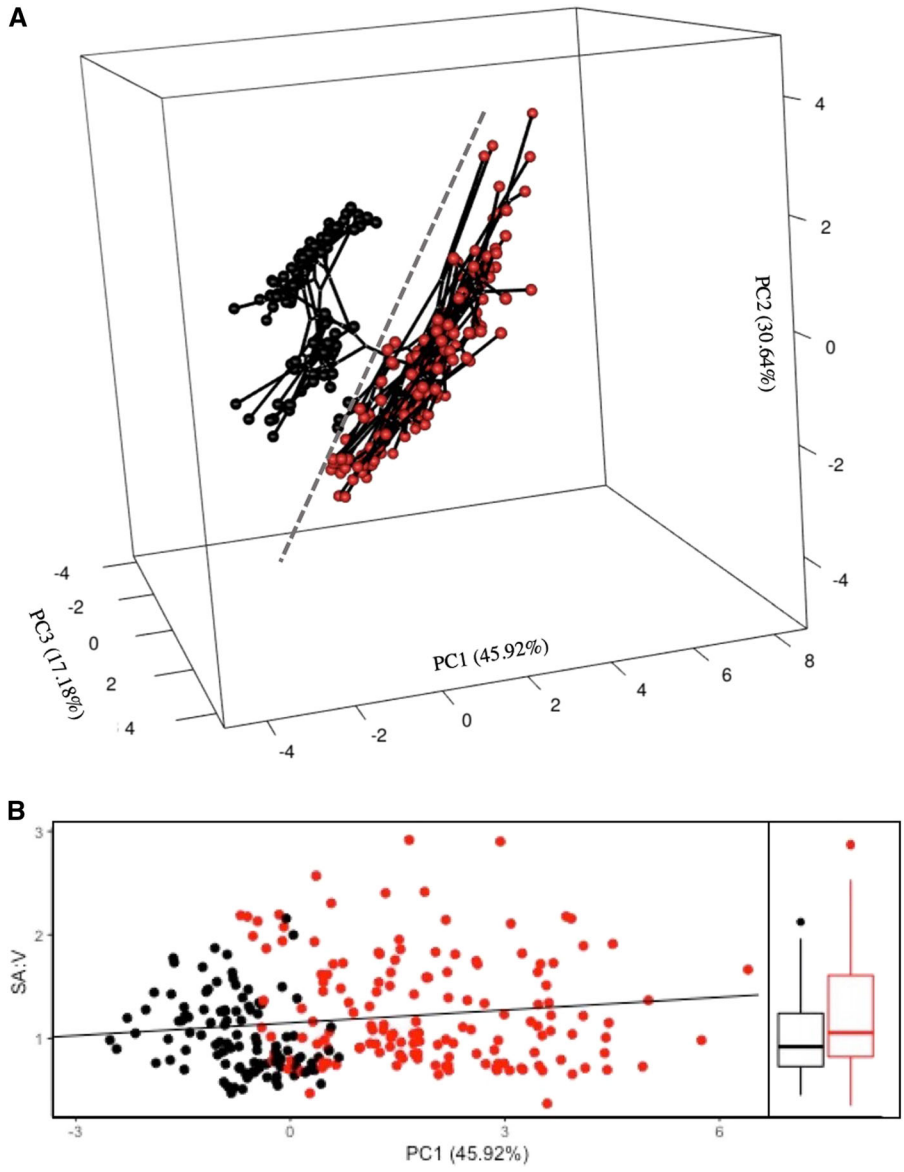


Figure 3. Panel A: Phyloclimatespace of PC axes 1, 2, and 3 representing 93.74% of the total measured climate variation. Tips represent species climate means standardized using normal deviates. This demonstrates a clear delineation between temperate (black) and tropical (red) species climates without overlap (grey dotted line). Additionally, the tropical species (red) climate means displayed over twice the climatic disparity as the temperate species (black) after taking phylogeny into consideration ($Disp_{Trop} = 0.279$, $Disp_{Temp} = 0.137$, $P = 0.001$). This mirrors the phyloclimatespace of *available* landscape (Fig. S2) that similarly shows greater climatic disparity in the tropics (7°S:56°N, 129°W:20°W). In panel B, SA:V is plotted against PC1, and the black line represents the significant linear regression estimate calculated by the phylogenetic ANCOVA ($P = 0.009$). The boxplot on the right side of Panel B summarizes the overall spread of SA:V values within each region, demonstrating the greater SA:V disparity in tropical species ($P = 0.001$).

desiccation rate), the positive correlation of SA:V with temperature refines the traditional understanding of how temperature influences desiccation in amphibians. Early empirical studies on salamander desiccation rates demonstrated that higher temperatures elicited higher desiccation rates (Spotila 1972), aligning with the consensus among herpetologists that plethodontids prefer cool environments (Petranka 1998). However, Spotila (1972) also demonstrated that these temperature effects were greatly diminished in humid conditions. In our study, the warm climates associated with higher SA:Vs across PC1 were also characterized by higher precipitation (Table 1); thus it seems probable that the detrimental effect of increased temperature on desiccation rate is mitigated by the concordant increase in precipitation. Further, dew point increases with temperature, allowing more water vapor to accumulate in the air in warmer temperatures (Ahrens 2000). Therefore, warmer and wetter climates likely provide

Table 2. ANCOVA table from climatic and regional PGLS analysis.

Variable	*F*	*Z*	*P*
PC1	8.8620	1.508	**0.009**
PC2	0.2545	−0.060	0.599
PC3	0.0016	−2.509	0.974
REGION	1.4759	0.755	0.220
PC1*REGION	0.2356	−0.124	0.637
PC2*REGION	0.5460	0.300	0.466
PC3*REGION	0.1907	−0.176	0.659

Only climate PC1 significantly correlated with SA:V (bolded). Interactions between PC axes were not included in the model as they are inherently orthogonal.

plethodontids with humid environments that allow for activity in exposed areas without risk of desiccation.

In this study, we presented strong evidence of a morphological response to ecological selective pressures in a family of salamanders whose morphology is not often associated with differences in habitat (Kozak and Wiens 2016). Previous investigations into the macroevolution of morphology have largely concluded that variation in plethodontid body proportions across taxa do not always correspond to what is predicted by selection across environmental gradients (Adams et al. 2009; Blankers et al. 2012; Baken and Adams 2019, but see Bonett and Blair 2017). The uniquely compelling results of our study suggest that SA:V may represent a key morphological trait that *does* respond predictably to environmental selective pressures, as much of the physiology of plethodontids, and thus their organismal performance, is mitigated through the consequences of cutaneous respiration and possible desiccation risk (see Feder 1983). This might also serve to explain why other measures of body shape have not shown predictable evolutionary patterns; parallel changes in SA:V can be accomplished by several different changes in body shape (e.g., lengthening either the torso or the tail both increase SA:V). Thus, different modifications of shape that confer similar SA:V adaptations could result in body shape evolution that does not appear to display a distinctive trajectory.

In addition, our novel SA:V estimation method provides advantages over the WH SA proxy. For instance, the WH proxy is based on two parameters (slope and intercept), which are treated as constants across all plethodontids. This approach explicitly assumes identical scaling across the 465 species in the family. As a consequence, the mass-based WH proxy neglects interspecific, intraspecific, and ontogenetic body shape variation in plethodontids as demonstrated by previous studies (e.g., Hanken 1982; Wake 1989; Adams et al. 2009). Consequently, the WH proxy does not accurately characterize SA:V, and thus the potential for error is high. By contrast, our novel method does account for body shape variation across individuals thereby characterizing allometric trends in SA:V should they be present. Furthermore, our method shows a 1:1 relationship with actual SA:Vs, indicating constancy in the accuracy of our measure (Fig. 2). Thus, our method is preferred and should be used in future investigations of SA:V in salamanders.

Our climatic analyses demonstrated the substantial impact of precipitation and temperature on the evolutionary history of Plethodontidae. Indeed, these results are in accord with previous studies that have shown these environmental variables influence ecology (e.g., Farallo et al. 2018), and our results illustrated the evolutionary impact of these climatic variables on morphology. This study therefore deepens our understanding of the role of these environmental variables in generating plethodontid diversity. We also suggest that future studies investigating how temperature and precipitation have impacted other facets of plethodontid evolution would be fruitful.

Finally, the results of our study shed new light on the unique evolutionary history of tropical salamanders. It has long been noted that the tropical plethodontid lineage represents an important and interesting radiation in amphibian evolution (Wake 1987). Namely, tropical plethodontids are known to have relatively divergent and fast evolving climatic niches (Kozak and Wiens 2007, 2010), a high prevalence of arboreality (McEntire 2016; Baken and Adams 2019), high rates of morphological evolution (Rabosky and Adams 2012), high rates of species diversification (Wiens 2007), and high species richness (AmphibiaWeb 2016). Although these patterns have interested biologists for years, attempts at explaining them have been narrow in scope, considering only a few observed patterns at a time. For instance, Rabosky and Adams (2012) implicated the high rate of morphological evolution as the mechanism behind increased tropical species richness. Others have suggested that the elevated diversification rates and greater species richness in tropical clades may be the result of either greater climatic stability across time (Wiens 2007) or faster rates of climatic niche evolution in the tropics (Kozak and Wiens 2010, 2016). Despite the many attempts to understand these phenomena in isolation, a single overarching explanation remains elusive. In this paper, we revealed several important relationships between climate, the tropics, and plethodontid morphology, which have the potential to provide a unifying pathway toward understanding the unique evolutionary history of tropical salamanders. Specifically, we argued that desiccation is a major constraint for salamander evolution, and responses to desiccation have driven the major ecological and evolutionary differences of temperate and tropical plethodontids. In this light, we hypothesize that the invasion of the Neotropics constituted a physiological release from desiccation, made possible by the inherently broader and less desiccation-prone climatespace available. We suggest that this relaxation of physiological selective pressures explains the increased disparity and rate of SA:V evolution, as well as

decreased extinction rates, the increased species richness, the faster morphological and climatic niche evolution, and the higher incidence of arboreality observed in the tropical clade. Through the lens of desiccation, many ecological and evolutionary patterns across regions can be explained as responses to relaxed physiological selective pressures offered by the tropical climatic landscape. Thus, we conclude that desiccation is one of the more impactful ecological and evolutionary forces for this family, through which many other regional patterns can be better understood.

AUTHOR CONTRIBUTIONS

EKB and DCA conceived of the study, EKB and LEM collected the data and conducted all analyses, and EKB and DCA contributed equally to the writing of the manuscript.

ACKNOWLEDGMENTS

We thank Bryan Juarez, Elizabeth Glynne, Rebekah Reynolds, Dr. Jordan Satler, Josh Justison, Dr. Joelle Barido-Sottani, and Dr. Nicole Valenzuela for comments on versions of the manuscript. This work was sponsored in part by the U.S. National Science Foundation grant DEB-1556379 to DCA and the 2017 SSB Graduate Student Research Award to EKB. We are grateful to D. Kizirian, T. Daeschler, J. Sites, L. Scheinberg, S. Rogers, C. Dillman, A. R. Resetar, L. McBrayer, K. Rowe, L. Welton, N. Camacho, S. Parker, J. Rosado, A. Nistri, C. Spencer, B. Stuart, C. Siler, B. Hollingsworth, T. Hibbitts, T. LaDuc, E. Braker, M. Nickerson, G. Schneider, K. de Queiroz, C. Franklin, G. Watkins-Colwell, and the staff from the following museums for loaning specimens for this research: American Museum of Natural History (AMNH), Academy of Natural Sciences of Philadelphia (ANSP), Brigham Young University Life Science Museum (BYU), California Academy of Sciences (CAS), Carnegie Museum of Natural History (CM), Cornell University Museum of Vertebrates (CUMV), Florida Museum of Natural History (FMNH), Georgia Southern University (GSU), Iowa State University (ISU), Biodiversity Institute at the University of Kansas (KU), Natural History Museum of Los Angeles County (LACM), Louisiana State University Museum of Natural Science (LSUMZ), Museum of Comparative Zoology (MCZ), Universitá Degli Studi Firenze Museo di Storia Naturale (MDSN), Museum of Vertebrate Zoology University of California, Berkley (MVZ), North Carolina State Museum of Natural Sciences (NCSM), Sam Noble Oklahoma Museum of Natural History University of Oklahoma (OMNH), San Diego Natural History Museum (SDNHM), Texas Cooperative Wildlife Collection (TCWC), Texas Natural History Collections (TNHC), University of Colorado Museum of Natural History (UCM), Florida Museum of Natural History (UF), University of Michigan Museum of Zoology (UMMZ), Smithsonian Institute National Museum of Natural History (USNM), University of Texas Arlington (UTA), and Peabody Museum of Natural History at Yale University (YPM).

DATA ARCHIVING

We provide an R script for a function to estimate SA:V using our method and the linear measures used to calculate SA:V species means for this study through the Dryad Digital Repository (https://doi.org/10.5061/dryad.59zw3r23m).

LITERATURE CITED

Adams, D. C. 2011. Quantitative genetic and evolution of head shape in *Plethodon* salamanders. Evol. Biol. 38:278–286.

———. 2014. Quantifying and comparing phylogenetic evolutionary rates for shape and other high-dimensional phenotypic data. Syst. Biol. 63:166–177.

Adams, D. C., C. M. Berns, K. H. Kozak, and J. J. Wiens. 2009. Are rates of species diversification correlated with rates of morphological evolution? Proc. R. Soc. B. 276:2729–2738.

Adams, D. C., M. L. Collyer, and A. Kaliontzopoulou. 2019. Geomorph: software for geometric morphometric analyses. R package version 3.1.0. https://cran.r-project.org/package=geomorph.

Ahrens, C. D. 2000. Essentials of meteorology: an invitation to the atmosphere, 3rd ed. Wadsworth Group: Brooks/Cole, Pacific Grove, CA.

AmphibiaWeb. 2016. University of California, Berkeley, CA, USA. Available at https://amphibiaweb.org.

Baken, E. K., and D. C. Adams. 2019. Macroevolution of arboreality in salamanders. Ecol. Evol. 9:7005–7016.

Beyer, W. H. 1981. CRC standard mathematical tables, 26th ed.CRC Press, Boca Raton, FL.

Blankers, T., D. C. Adams, and J. J. Wiens. 2012. Ecological radiation with limited morphological diversification in salamanders. J. Evol. Biol. 25:634–646.

Blomberg, S. P., T. Garland Jr, and A. R. Ives. 2003. Testing for phylogenetic signal in comparative data: behavioral traits are more labile. Evolution 57:717–745.

Bonett, R. M., and A. L. Blair. 2017. Evidence for complex life cycle constraints on salamander body form diversification. Proc. Natl. Acad. Sci. USA 114:9936–9941.

Collyer, M. L., and D. C. Adams. 2018. RRPP: An R package for fitting linear models to high-dimensional data using residual randomization. Methods Ecol. Evol. 9:1772–1779.

———. 2019. RRPP: linear model evaluation with randomized residuals in a permutation procedure. https://cran.r-project.org/web/packages/RRPP.

Constable, H., R. P. Guralnick, J. Wieczorek, C. Spencer, and A. T. Peterson. 2010. VertNet: a new model for biodiversity data sharing. PLoS Biol. 8:e1000309.

Currie, D. J. 1991. Energy and large-scale patterns of animal- and plant-species richness. Am. Nat. 137:27–49.

Emlen, D. J., L. C. Lavine, and B. Ewen-Campen. 2007. On the origin and evolutionary diversification of beetle horns. Proc. Natl. Acad. Sci. USA 104:8661–8668.

Farallo, V. R., R. Wier, and D. B. Miles. 2018. The bogert effect revisited: salamander regulatory behaviors are differently constrained by time and space. Ecol. Evol. 8:11522–11532.

Feder, M. E. 1983. Integrating the ecology and physiology of plethodontid salamanders. Herpetologica 39:291–310.

Feder, M. E., and P. L. Londos. 1984. Hydric constraints upon foraging in a terrestrial salamander, *Desmognathus ochrophaeus* (Amphibia: Plethodontidae). Oecologia 64:413–418.

Ficetola, G. F., E. Lunghi, C. Canedoli, E. Padoa-Schioppa, R. Pennati, and R. Manenti. 2018. Differences between microhabitat and broad-scale patterns of niche evolution in terrestrial salamanders. Sci. Rep. 8:10575.

Fick, S. E., and R. J. Hijmans. 2017. Worldclim 2: new 1-km spatial resolution climate surfaces for global land areas. Int. J. Climatol. 37:4302–4315.

Fisher-Reid, M. C., K. H. Kozak, and J. J. Wiens. 2012. How is the rate of climatic-niche evolution related to climatic-niche breadth? Evolution 66:3836–3851.

Fraser, D. F. 1976. Empirical evaluation of the hypothesis of food competition in salamanders of the genus plethodon. Ecology 57:459–471.

Gade, M. R., and W. E. Peterman. 2019. Multiple environmental gradients influence the distribution and abundance of a key forest-health indicator species in the Southern Appalachian Mountains, USA. Landsc. Ecol. 34:569–582.

Gifford, M. E. 2016. Physiology of plethodontid salamanders: a call for increased efforts. Copeia 104:42–51.

Gomez-Rodriguez, C., A. Baselga, and J. J. Wiens. 2015. Is diversification rate related to climatic niche width? Global Ecol. Biogeogr. 24:383–395.

Grigg, J. W., and L. B. Buckley. 2013. Conservatism of lizard thermal tolerances and body temperatures across evolutionary history and geography. Biol. Lett. 9:20121056.

Hanken, J. 1982. Appendicular skeletal morphology in minute salamanders, genus *Thorius* (Amphibia: Plethodontidae): growth regulation, adult size determination, and natural variation. J. Morphol. 174:57–77.

Hoekstra, H. E., J. G. Krenz, and M. W. Nachman. 2004. Local adaptation in the rock pocket mouse (*Chaetodipus intermedius*): natural selection and phylogenetic history of populations. Heredity 94:217.

IUCN. 2010. IUCN Red List of Threatened Species Database Version 2010. Available at www.iucnredlist.org. Accessed June 20, 2019.

Kozak, K. H., and J. J. Wiens. 2007. Climatic zonation drives latitudinal variation in speciation mechanisms. Proc. R. Soc. B. 274:2995–3003.

———. 2010. Accelerated rates of climatic-niche evolution underlie rapid species diversification. Ecol. Lett. 13:1378–1389.

———. 2016. What explains patterns of species richness? The relative importance of climatic-niche evolution, morphological evolution, and ecological limits in salamanders. Ecol. Evol. 6:5940–5949.

Lane, J. E., D. L. Swanson, R. M. Brigham, and A. E. McKechnie. 2004. Physiological responses to temperature by whip-poor-wills: more evidence for the evolution of low metabolic rates in Caprimulgiformes. Condor 106:921–925.

Losos, J. 1992. The evolution of convergent structure in Caribbean Anolis communities. Syst. Biol. 41:403–420.

MacMahon, J. A. 1964. Factors influencing the rate of water loss in salamanders. Am. Zool. 40:159–171.

McEntire, K. D. 2016. Arboreal ecology of plethodontidae: a review. Copeia 104:124–131.

McEntire, K. D., and J. C. Maerz. 2019. Integrating ecophysiological and agent-based models to simulate how behavior moderates salamander sensitivity to climate. Front. Ecol. Evol. 7:22.

Moodie, G. E. E. 1972. Predation, natural selection and adaptation in an unusual threespine stickleback. Heredity 28:155.

O'Meara, B. C., C. Ané, M. J. Sanderson, and P. C. Wainwright. 2006. Testing for different rates of continuous trait evolution using likelihood. Evolution 60:922–933.

Peterman, W. E., and R. D. Semlitsch. 2014. Spatial variation in water loss predicts terrestrial salamander distribution and population dynamics. Oecologia 176:357–369.

Petranka, J. W. 1998. Salamanders of the United States and Canada. Smithsonian Institution Press, Washington, DC.

R Core Team. 2018. R: a language and environment for statistical computing. Version 3.5.0. R Foundation for Statistical Computing, Vienna. Available at http://cran.R-project.org.

Rabosky, D. L., and D. C. Adams. 2012. Rates of morphological evolution are correlated with species richness in salamanders. Evolution 66:1807–1818.

Ray, C. 1958. Vital limits and rates of desiccation in salamanders. Ecology 39:75–83.

Riddell, E. A., and M. W. Sears. 2015. Geographic variation of resistance to water loss within two species of lungless salamanders: implications for activity. Ecosphere 6:1–16.

Riedel, B. L., K. R. Russell, and W. M. Ford. 2012. Physical condition, sex, and age-class of Eastern Red-Backed Salamanders (*Plethodon cinereus*) in forested and open habitats of West Virginia, USA. Int. J. Zool. 2012:1–8.

Rittenhouse, T. A., M. C. Doyle, C. R. Mank, B. B. Rothermel, and R. D. Semlitsch. 2004. Substrate cues influence habitat selection by spotted salamander. J. Wildl. Manage. 68:1151–1158.

Sattler, P., and N. Reichenbach. 1998. The effects of timbering on *Plethodon hubrichti*: short-term effects. J. Herpetol. 32:399–404.

Schluter, D., and J. D. McPhail. 1992. Ecological character displacement and speciation in sticklebacks. Am. Nat. 140:85–108.

Shen, X. X., D. Liang, M. Y. Chen, R. L. Mao, D. B. Wake, and P. Zhang. 2016. Enlarged multilocus data set provides surprisingly younger time of origin for the Plethodontidae, the largest family of salamanders. Syst. Biol. 65:66–81.

Spight, T. M. 1968. The water economy of salamanders: evaporative water loss. Physiol. Zool. 41:195–203.

Spotila, J. R. 1972. Role of temperature and water in the ecology of lungless salamanders. Ecol. Monogr. 42:95–125.

Spotila, J. R., and E. N. Berman. 1976. Determination of skin resistance and the role of the skin in controlling water loss in amphibians and reptiles. Comp. Biochem. Physiol. 55A:407–411.

Title, P. O., and J. B. Bemmels. 2018. ENVIREM: an expanded set of bioclimatic and topographic variables increases flexibility and improves performance of ecological niche modeling. Ecography 41:291–307.

Ultsch, G. R. 1976. Respiratory surface area as a factor controlling the standard rate of O_2 consumption of aquatic salamanders. Respir. Physiol. 26:357–369.

Wainwright, P. C. 1988. Morphology and ecology: functional basis of feeding constraints in Caribbean labrid fishes. Ecology 69:635–645.

Wake, D. B. 1987. Adaptive radiation of salamanders in middle American cloud forests. Ann. Mo. Bot. Gard. 74:242–264.

———. 1989. Phylogenetic implications of ontogenetic data. Geobios 22:369–378.

Whitford, W. G., and V. H. Hutchinson. 1967. Body size and metabolic rate in salamanders. Physiol. Zool. 40:127–133.

Wiens, J. J. 2007. Global patterns of diversification and species richness in amphibians. Am. Nat. 170:S86–106.

Associate Editor: S. Patek
Handling Editor: M. R. Servedio

Supporting Information

Additional supporting information may be found online in the Supporting Information section at the end of the article.

Table S1. Description of 11 linear measurements collected on each specimen from which SA:V was estimated.
Figure S1. Linear regression of the log transformed WH proxy against empirical SA:Vs measured across 21 individual specimens.
Figure S2. Landscape climatespace with convex hulls for each region.
Figure S3. F values calculated for each term of the ANCOVA model across the 1000 posterior chronograms from the phylogenetic reconstruction provided by Bonett and Blair 2017.
Figure S4. Tropical/temperate ratios of SA:V morphological disparity and evolutionary rate calculated across the 1000 posterior chronograms from the phylogenetic reconstruction provided by Bonett and Blair 2017.
Table S2. Species summaries of climatic variables and regional classification.
Table S3. Specimens measured for SA:V species means calculated in this study (see Supporting Information excel file).